

Improvement of MCDI operation and design through experiment and modelling: Regeneration with brine and optimum residence time



Armineh Hassanvand^a, George Q. Chen^b, Paul A. Webley^a, Sandra E. Kentish^{b,*}

^a Department of Chemical and Biomolecular Engineering, University of Melbourne, Parkville, VIC 3010, Australia

^b The ARC Dairy Innovation Hub, Department of Chemical and Biomolecular Engineering, University of Melbourne, Parkville, VIC 3010, Australia

ARTICLE INFO

Keywords:

Membrane capacitive deionization

Brine regeneration

Water recovery

ABSTRACT

Membrane Capacitive Deionization (MCDI) is an energy efficient, electrochemical desalination technology, in which ions are removed from a salty stream upon applying a constant voltage or current. The ions are stored in carbon electrodes and then released back into the stream by reversing the polarity. In this work, we aimed to assess the feasibility of using a brine stream to regenerate the MCDI unit in order to improve water recovery. We further aimed to determine the optimum residence time in the MCDI unit. To achieve these objectives, we first enhanced the ion transport model previously developed for MCDI by independently measuring the counter-ion and co-ion diffusion coefficients in the ion-exchange membranes. These experiments allowed for an asymmetric model of the MCDI unit where the voltage drop across the cation exchange membrane was greater than that across the anion exchange membrane. Using this revised model, we found that in batch operation, a brine to feed water concentration ratio of around two was optimum. In continuous operation, over 40% enhancement in water recovery could be achieved when the regeneration brine was partially recycled, but water productivity dropped. We further showed that the maximum desalination capacity did not increase beyond a critical residence time in the MCDI cell, while the water recovery decreased.

1. Introduction

Desalination of sea and brackish water has become more common over the past decades to meet freshwater requirements for domestic, agricultural and industrial demands. Desalination capacity, energy demand, regeneration method and water recovery are the main features distinguishing the technologies developed for this purpose, which are generally thermally or membrane based [1,2]. Capacitive Deionization (CDI) is an alternative, electrochemical water treatment method in which ions are temporarily adsorbed in electrical double layers of two oppositely charged porous carbon electrodes [3]. Therefore the desalination capacity is reliant on the carbon material used in the electrode fabrication [4,5]. To enhance the performance of CDI, Membrane Capacitive Deionization (MCDI) has also been proposed, where ion-exchange membranes (IEMs) are placed in front of the charged electrodes to inhibit the co-ions, i.e. ions carrying the same charge as the surface, from reaching the electrodes [6,7]. In CDI or MCDI, ions or other charged species are removed from the concentrated feed. However, this is not the case for most other desalination technologies in which water is separated from the polluted stream. It is thus apparent that at lower concentrations of the charged species in comparison with

that of water, the energy consumption of CDI based processes will be significantly lower than the latter [8]. Therefore, CDI or MCDI is mostly employed as an energy-efficient method for brackish water remediation where the salinity is limited to 1000 mg L^{-1} [9].

Once the carbon pores reach their saturation limit, the CDI or MCDI unit is not capable of adsorbing ions anymore. Therefore, a regeneration step is required to deplete the electrode materials of the charged species. In CDI, the previously adsorbed ions are released back to the liquid phase by dropping the system voltage to zero, while in MCDI it is more common to release these ions by reversing the polarity. As a result the stack undergoes repetitive adsorption/desorption cycles [10]. Ease of regeneration adds to the merits of this promising desalination method [11].

While many attempts have been made towards synthesis of novel carbon materials with improved physico-chemical properties for CDI processes [12,13], less research has been conducted on the operational aspects of both CDI and MCDI. Zhao et al. [14] were the first to optimize the salt adsorption in MCDI by varying operational variables within both constant voltage and constant current modes. Recently, García-Quismondo et al. [15] considered new operational modes to increase energy efficiency in CDI by varying charge and discharge

* Corresponding author at: Department of Chemical and Biomolecular Engineering, The University of Melbourne, Parkville, 3010, Victoria, Australia.
E-mail address: sandraek@unimelb.edu.au (S.E. Kentish).

current densities and also investigated the use of a concentrated brine stream during discharge. Yet more research is needed to improve the design aspects of MCDI. To illustrate, feed water recovery, i.e. the volumetric ratio of desalinated water produced to that of the feed water, is one such operational metric used to evaluate water treatment processes [16]. In the field of MCDI, the higher the feed water recovery, the less feed water volume is wasted during the desorption step. In this work, we specifically consider the potential of regenerating the MCDI unit with a stream of higher salt concentration than the feed to increase the feed water recovery. Since this is a very critical question, more exploration is required to determine its feasibility especially in the presence of ion-exchange membranes. If a more concentrated stream can be utilised in the desorption step, a certain amount of the water for regeneration can be recycled a number of times which then leads to much greater water recovery.

In this paper, we explore this concept using both experimental techniques and a theoretical model. The modified Donnan Theory developed by Biesheuvel et al. [17,18] is the most well developed model available in the literature to describe the storage of ions in the EDLs of micropores (< 2 nm) of carbon electrodes. The same research group has also proposed a dynamic ion transport model to describe the performance of the MCDI unit [17,19,20]. Tang et al. [21] has recently used a similar approach to model the removal of fluoride in CDI. This ion transport model includes all the mass and charge balances throughout the MCDI unit and is combined with modified Donnan theory to describe the ion storage in the electrical double layers (EDLs). Nonetheless, this theoretical method is based on various simplifying assumptions. In this work we avoid some of these assumptions by (i) measuring the diffusion coefficients in the ion-exchange membranes; (ii) using these values to adjust the voltage distribution across the two half-cells and (iii) including the ion activity coefficient in the solution and the membrane phases. The novel features introduced into the mathematical approach strengthen the model, as estimation of some parameters is replaced with direct measurements. The improved ion transport model was then utilised to determine the impact of partially recycling the regeneration brine, and further to determine the optimum residence time in the MCDI unit.

2. MCDI model

To describe the deionization process the modified Donnan (mD) Theory proposed by Biesheuvel et al. [18] is used to describe the ion storage in the electrical double layers (EDLs) of the carbon electrode (Section 2.1). Mass transfer equations then enable the prediction of the ion flux from the flow channel formed by a spacer through the ion-exchange membranes to access these EDLs (Section 2.2). In this approach, the effect of faradaic reactions and also the contribution of hydronium and hydroxyl ions have been neglected. Fig. 1 gives an overview of the MCDI arrangement of one of two half-cells that is described by the model. While macro and micro-pores are distributed within the carbon electrode, to better demonstrate the concentration and potential drop, they are drawn in series in Fig. 1.

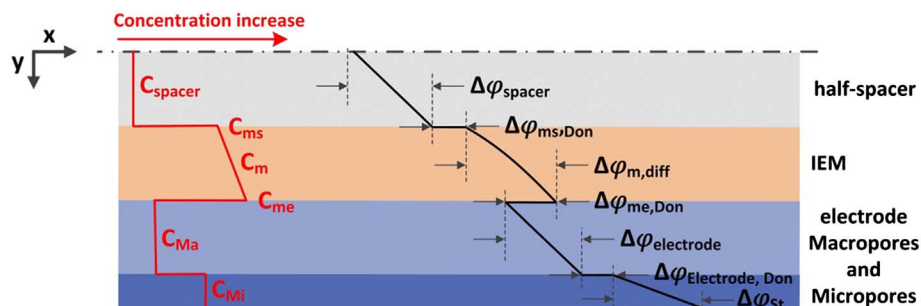


Fig. 1. Schematic illustration of counter-ion concentration (C) and dimensionless voltage (ϕ) distribution over a half-cell.

2.1. Modified Donnan theory in the micropores

Modified Donnan theory uses the Boltzmann distribution to correlate the concentration in the micropores of the carbon where a surface charge is applied, to that of the macropores where the concentration of anions and cations is identical. A term μ_{att} is introduced to account for the physical adsorption of ion i onto the carbon surface at zero voltage (Eq. (1)) [17]:

$$C_{i,Mi} = C_{Ma} \cdot \exp(-z_i \cdot \Delta\phi_{electrode,Don} + \mu_{att}) = C_{Ma} \cdot \exp(-z_i \cdot \Psi / V_T + \mu_{att}) \quad (1)$$

where $C_{i,Mi}$ is the concentration of ion i in the micropores of the carbon, C_{Ma} is the salt concentration in the macropores, and z_i is the valency of ion type i , $\Delta\phi_{electrode,Don}$ is the Donnan potential difference, which in turn can be expressed in terms of the electrical potential difference (Ψ) between the macro and micro pores, and the thermal voltage $V_T = k_B T / e$ (≈ 25.5 mV at room temperature), where e is the electrical charge of an electron, k_B is the Boltzmann constant and T is the absolute temperature [18]. In contrast to the conventional EDL model of Gouy-Chapman-Stern where a distribution of the electrical potential is considered inside the pores, modified Donnan Theory considers $\Delta\phi_{electrode,Don}$ as a constant. The reason behind this assumption is that the micropore size within the carbon material used is commonly small enough to result in overlapping EDLs.

The charge concentration ($C_{charge,Mi}$) is defined as the difference between the concentration of cations in the micropores with that of the anions. For a monovalent salt, $C_{charge,Mi}$ can be calculated from Eq. (2) as

$$C_{charge,Mi} = C_{cation,Mi} - C_{anion,Mi} = -2 \cdot C_{Ma} \cdot \exp(\mu_{att}) \cdot \sinh(\Delta\phi_{electrode,Don}) \quad (2)$$

According to the modified Donnan Theory [22], this charge concentration is proportional to the Stern layer potential difference ($\Delta\phi_{St}$) as Eq. (3).

$$\Delta\phi_{St} \cdot V_T \cdot (C_{St,0} + \alpha \cdot C_{charge,Mi}^2) = -F \cdot C_{charge,Mi} \quad (3)$$

where F is the Faraday constant, $C_{St,0}$ is the Stern layer capacitance at zero voltage and α demonstrates the charge dependency of the Stern layer capacity.

2.2. Dynamic ion transport model of MCDI

During the adsorption step, the salt concentration falls along the direction of the flow in the MCDI unit as the ions are being removed from the bulk stream. Neglecting axial dispersion, one can write Eq.(4) to describe the concentration in the spacer compartment (C_{spacer})

$$\frac{\partial C_{spacer}}{\partial t} = -v \cdot \frac{\partial C_{spacer}}{\partial x} - \frac{j_{iy}}{\delta_{spacer}} \quad (4)$$

where δ_{spacer} is the thickness of the spacer which defines the flow channel width, v is the velocity in the flow channel and j_{iy} is the flux of ion type i moving in direction y , perpendicular to the flow direction, to reach the ion-exchange membrane. Assuming a quasi-steady-state

condition for the ion-exchange membrane, the flux of ions leaving the flow channel equals the flux passing through the ion-exchange membrane, which is identical to the flux of ions entering the electrode. In the absence of convective flow, the flux of ion i through the membrane is composed of two terms: diffusion flux due to the chemical potential gradient, and electromigration due to the electrical potential gradient [23,24]. Therefore, j_{iy} can be written as

$$j_{iy} = -D_{i,m} \left(\frac{\partial C_{i,m}}{\partial y} + \bar{C}_{i,m} \frac{\partial \ln \gamma_{i,m}}{\partial y} + z_i \bar{C}_{i,m} \frac{\partial \varphi_m}{\partial y} \right) \quad (5)$$

where D_i is the diffusivity coefficient and γ_i is the activity coefficient of ion i . Subscript m refers to the values within the membrane, while the overbar indicates the average concentration within the membrane.

Since the membrane is assumed to be in equilibrium with the adjacent solution, one can write the equality of chemical potentials of dissociated monovalent ions in both phases, i.e. membrane and the adjacent solution [23]. For instance, at the membrane/spacer interface we obtain

$$a_{+,m} \cdot a_{-,m} = a_{+,spacer} \cdot a_{-,spacer} \quad (6)$$

where a is the activity of each ion.

It is noteworthy that the activity coefficient of the counter-ions in an ion-exchange membrane is significantly lower than that of the free aqueous solution [25]. This is because of the high concentration of the counter-ions within this phase and the electrostatic interaction between the counter-ions and fixed charges in the structure of the ion-exchange polymer [26]. Since the concentration of co-ions in the membrane is much lower than that of counter-ions, the activity coefficient of these ions does not exhibit as significantly non-ideal behavior as the counter-ions. However, the value in the IEM is still smaller than that in the bulk solution. The activity coefficient of the counter and co-ions in the IEM is determined using Manning's counter-ion condensation theory (See Appendix. A) [26].

Given the need for electroneutrality in the ion-exchange membrane with $C_{fix,m}$ as the concentration of fixed charges (the concentrations of counter-ion and co-ion within the membrane on the spacer side can be determined by solving Eq. (7) simultaneously with Eq. (6).

$$\sum_i z_i \cdot C_{i,m} + z_{fix} \cdot C_{fix,m} = 0 \quad (7)$$

where $C_{fix,m}$ is the concentration of fixed charges within the membrane.

As discussed earlier, the ions enter the carbon electrode consisting of macro and micro pores with different volume fractions. An ion mass balance inside the electrode results in

$$\frac{\partial}{\partial t} (\varnothing_{Ma} \cdot C_{Ma} + \varnothing_{Mi} \cdot C_{i,Mi}) = \frac{j_{iy}}{\delta_{electrode}} \quad (8)$$

where \varnothing is the volume fraction, and $\delta_{electrode}$ is the thickness of the carbon layer. Subscripts Ma and Mi refer to the macro and micro-pores of the electrode, respectively.

The accumulation of $C_{charge,Mi}$ in the micropores as a function of current density passing through the unit (I) is expressed by

$$\frac{\partial}{\partial t} (\varnothing_{Mi} \cdot C_{charge,Mi}) = \frac{I}{F \cdot \delta_{electrode}} \quad (9)$$

2.3. Potential differences

As shown in Fig. 1, there are several potential drops across the system, including across the spacer filled flow channel, at the membrane interfaces, within the membrane, across the macropores in the porous electrode and inside the electrical double layer of the micropores. The sum of these values equals the applied potential, in the case of no external resistance. In the following part we describe the potential drops over each compartment.

The potential drop over half of the spacer filled flow channel is a

linear function of the current density according to

$$V_T \cdot \frac{\partial \varphi_{spacer}}{\partial y} \approx V_T \cdot \frac{2 \Delta \varphi_{spacer}}{\delta_{spacer}} = -\frac{I}{\kappa_{spacer}} = -V_T \cdot \frac{I}{F \sum_i z_i^2 \cdot C_i \cdot D_i} \quad (10)$$

where κ_{spacer} is the ionic conductivity in the flow channel, which can be expressed as $F \sum_i z_i^2 \cdot C_i \cdot D_i$, and D is the effective diffusion coefficient of ion i [27]. Values of $1.33 \times 10^{-9} \text{ m}^2 \text{ s}^{-1}$ and $2.03 \times 10^{-9} \text{ m}^2 \text{ s}^{-1}$ can be used for the diffusion coefficient of Na^+ and Cl^- in an aqueous solution, respectively [28]. Considering the flow channel is thin, we can use the linear approximation as shown Eq.(10).

The ion-exchange membrane is placed between two solutions of the same electrolytes at different concentrations. The membrane potential difference ($\Delta \varphi_m$) in such a system consists of a diffusion potential difference ($\Delta \varphi_{m,diff}$) within the membrane and the Donnan potentials at the interfaces as

$$\Delta \varphi_m = \Delta \varphi_{m,diff} + \Delta \varphi_{ms,Don} + \Delta \varphi_{me,Don} \quad (11)$$

where $\Delta \varphi_{ms,Don}$ and $\Delta \varphi_{me,Don}$ are the Donnan potentials attained at the spacer/membrane and membrane/electrode macropore interfaces, respectively [23]. These can be described by Eq. (12) and (13):

$$\Delta \varphi_{ms,Don} = -\frac{1}{z_i} \cdot \ln \frac{C_{i,ms} \cdot \gamma_{i,ms}}{C_{i,spacer} \cdot \gamma_{i,spacer}} \quad (12)$$

$$\Delta \varphi_{me,Don} = -\frac{1}{z_i} \cdot \ln \frac{C_{i,Ma} \cdot \gamma_{i,Ma}}{C_{i,me} \cdot \gamma_{i,me}} \quad (13)$$

$C_{i,ms}$ is the concentration of ion i at the membrane interface with the spacer, while $C_{i,me}$ is the concentration of ion i at the membrane interface with the electrode macropores.

Furthermore, the diffusion-related potential term in Eq. (11) is related to the current density by

$$V_T \cdot \frac{\partial \varphi_{m,diff}}{\partial y} = -\frac{I}{\kappa_m} \quad (14)$$

where κ_m is the electrical conductivity of the cation/anion selective membrane (S m^{-1}) [27]. Assuming the potential difference across the membrane to be linear, we obtain

$$\frac{\Delta \varphi_{m,diff}}{\delta_m} = -\frac{I}{F \cdot D_{i,m} \cdot \bar{C}_{i,m}} \quad (15)$$

where $\bar{C}_{i,m}$ is the arithmetic average of the ion i concentration at the two membrane interfaces. Using Eqns. (11) to (15), the potential drop over the respective cation and anion exchange membranes can be calculated individually.

The equivalent conductance of the solution within the macropores participating in the voltage drop across the electrode is given by Eq. (16) [29]

$$V_T \cdot \frac{\Delta \varphi_{electrode}}{\delta_{electrode}} = -\frac{I}{\kappa_{electrode}} \quad (16)$$

Finally, the distribution of voltage across all the layers and interfaces can be described by:

$$\frac{V_{Cell}}{V_T} + 2 \Delta \varphi_{spacer} + \Delta \varphi_{CEM} + \Delta \varphi_{AEM} + 2 \Delta \varphi_{electrode} + 2(\Delta \varphi_{electrode,Don} + \Delta \varphi_{St})_{EDL} = 0 \quad (17)$$

where V_{Cell} is the electrical voltage applied across the cell and $\Delta \varphi_{electrode,Don}$ and $\Delta \varphi_{St}$ are as defined in Section 2.1.

2.4. MCDI unit discretisation

The equations above divide the unit into two asymmetric half-cells perpendicular to the flow direction. To account for dispersion effects, the electrode unit is also divided into N sub-cells in the direction of flow. Then, for each sub-cell k and time step Δt , we find the relationship

between the concentration in the flow channel ($C_{spacer,k}$), the ion transport rate through the membrane and the ion storage rate in the carbon micropores as a function of time (t). As each sub-cell is considered as an ideal mixed flow reactor, Eq.(4) can be expressed as Eq. (18):

$$\frac{(C_{spacer,k,t} - C_{spacer,k,t-1})}{\Delta t} = -\frac{N}{t_{spacer}} (C_{spacer,k,t} - C_{spacer,k-1,t}) - \frac{j_{iy,k,t}}{\delta_{spacer}} \quad (18)$$

where k is the sub-cell number, running from 1 for the inlet, to $(N + 1)$ for the effluent, and Δt is a time step of 10 s between $t-1$ and t . The residence time in the flow channel is given by \bar{t}_{spacer} . The time step should be selected small enough that its further reduction does not affect the modelling results. Eqs. (1), (4), (8), (9), and (17) are solved simultaneously to find $C_{spacer,k,t}$ in mol m⁻³ in the k^{th} sub-cell at time t .

3. Materials and methods

3.1. Materials

The analytical grade of all chemicals was utilised. Polyvinylidene fluoride (PVDF, Mw ~530,000 g mol⁻¹, Sigma-Aldrich), N–N dimethylformamide (DMF, 99.8%, Merck Millipore) and activated carbon (AC Norit SA 4, Cabot Norit Activated Carbon, USA) were utilised for electrode preparation. Sodium chloride (NaCl, 99.7%, ChemSupply) was used to prepare salt solutions at different concentrations. Sodium hydroxide (NaOH, 97.0%, ChemSupply), hydrochloric acid (HCl, 37.0%, ChemSupply), caesium chloride (CsCl, 99.9%, Sigma Aldrich) and sodium iodide (NaI, 99.0%, Ajax FineChem) were used for membrane characterization. Solutions were prepared using water with minimum electrical resistance of 18.2 MΩ cm (MilliQ, Millipore).

3.2. MCDI set-up

To prepare the porous carbon electrodes, PVDF was dissolved in DMF at 100 °C. Powdered activated carbon was then added to the mixture in a mass ratio of AC to PVDF of 1:10. Following 2 h of mixing and evaporation of excess solvent, the dense slurry was then cast on a graphite sheet (DSN 530, Suzhou Dasen Electronics Material Co., China) as a current collector. The electrode was placed in a fan-forced oven at 110 °C overnight and then in a vacuum oven at 80 °C for 2 h to fully evaporate the remaining solvent. The carbon electrode was characterised by scanning electron microscopy, surface area and pore size analysis and cyclic voltammetry. These details can be found in Appendix B.

The capacitive deionization cell was formed from two 10 cm by 20 cm electrodes with a narrow channel of 0.3 cm by 8 cm cut into one end of each to allow for water entry and exit. Each electrode carries a carbon mass of 6.5 ± 0.5 mg cm⁻² with an average thickness of 150 ± 15 μm. As a MCDI cell, cation and anion exchange membranes (Neosepta CMX, thickness of 170 μm, and Neosepta AMX, thickness of 140 μm) were introduced in front of the negatively and positively charged electrodes, respectively. To prevent short circuiting and to form the flow channel, the 0.9 mm gap between the membranes was filled with a non-conductive spacer (Low Foulant spacer 34 mil, Sterlitech). A poly(carbonate) frame maintained all the layers in place. A DC power module (N6731B, Agilent) in a modular power system mainframe (N6700B, Agilent) was employed to apply a constant electrical voltage and also monitor the current passing through the unit. A peristaltic pump (NEMA 4 ×, Watson Marlow) was used to control the flow rate of the feed. The data measured by conductivity and pH probes (S470-kit, Mettler Toledo) was recorded to a laboratory computer. A schematic diagram of the MCDI set-up and all the layers within the MCDI cell are provided in Appendix C. (See Fig. C1).

3.3. Membrane characterization

The permeability of the counter-ions through the ion-exchange membrane was measured directly. In this approach, a membrane coupon was clamped between two chambers of a glass diffusion device (PermeGear Side-Bi-Side cell, USA). For the CMX cation exchange membrane, one chamber was filled with NaCl solution while the other was filled with HCl of the same concentration. The membrane was pre-soaked in the same NaCl solution for 48 h to reach equilibrium. By monitoring the pH values in the salt solution chamber as a function of time, the number of H⁺ ions transferred can be determined, which due to electroneutrality must be identical to that of Na⁺ ions travelling in the opposite direction. From the rate at which H⁺ is transferred, the permeability of Na⁺ ($P_{+,m}$) can be obtained from Eq.(19) [30], as the mobility of Na⁺ is much less than that of H⁺ and hence is rate limiting.

$$\ln \left(1 - 2 \frac{C_{H^+}^{Salt\ side}(t)}{C_{H^+}^{Acid\ side\ initial}} \right) = -2 \frac{A}{V \cdot \delta_m} \cdot P_{+,m} \cdot t \quad (19)$$

where $C_{H^+}^{Salt\ side}$ and $C_{H^+}^{Acid\ side\ initial}$ are concentration of H⁺ ions in salt solution chamber and the initial concentration of H⁺ ions in acid solution, respectively, A is the orifice area, V is the volume of each chamber, and t is time. A similar experiment was carried out to study the anion exchange membrane, AMX, where NaCl and NaOH solutions of the same concentration were used to exchange counter-ions. The temperature was kept constant at 23 ± 2 °C; hence, pK_w was taken as constant at 14.

Similarly, the permeability of co-ions through CMX and AMX can be measured by replacing the acid and base solutions with water. In this case, to maintain electroneutrality, each co-ion transferring from the salt chamber is accompanied by a counter-ion. The salt concentration increase in the water chamber is measured by a conductivity probe. The permeability of the co-ion can then be determined using a similar equation to Eq. (20) by substituting C_{H^+} with C^{sol} and $P_{+,m}$ with $P_{-,m}$.

In another set of experiments, the concentration of fixed charges ($C_{fix,m}$), the counter-ion partition coefficient ($K_{+,m}$) and that of the co-ion ($K_{-,m}$) of the same membrane was measured by the method recently proposed by Kamcev et al. [26]. In brief, a circular piece of membrane was first equilibrated at the same NaCl concentration (C^{sol}) as that used for the permeability measurements described above. The volume of the swollen membrane disk (V_m) was determined by measuring its diameter and thickness. The CMX membrane was then moved to a solution of CsCl at higher concentration to release the adsorbed sodium and uptake caesium ions; conversely, the AMX membrane was moved to a concentrated NaI solution to exchange adsorbed chloride in the membrane matrix with iodide ions. Knowing the swollen volume of the membrane, the partition coefficient can be obtained as the ratio of counter-ion concentration in the swollen membrane to that of the solution as Eq. (20)

$$K_{\pm,m} = \frac{(C_{\pm final}^{external} \cdot V^{external})}{C^{sol} \cdot V_m} \quad (20)$$

where $C_{\pm final}^{external}$ refers to the final concentration of the counter-ion in either CsCl or NaI solutions and V is the volume. As it is generally known that $P_{+,m} = D_{+,m} \cdot K_{+,m}$, one can then determine the diffusivity coefficient of the counter-ion diffusing through the membrane which is used during modelling in Eqs. (5) and (15).

It is apparent that the concentration of counter-ions in the membrane ($C_{+,m}$) can be calculated from Eq. (21)

$$C_{\pm,m} = \frac{(C_{\pm final}^{external} \cdot V^{external})}{V_m} \quad (21)$$

On the other hand, the concentration of co-ions in the membrane ($C_{-,m}$) can be obtained by replacing the external solution with DI water. In other words, the membrane which has been equilibrated with

NaCl solution is then moved to DI water to release the adsorbed co-ions back into water. Therefore, Eqs. (20) and (21) can be used to determine the partition coefficient and concentration of both types of ions in the membrane. The diffusivity coefficient of the co-ion can be determined similarly from $P_{-,m} = D_{-,m} \cdot K_{-,m}$. The outcome of this experiment, i.e. determination of counter and co-ions concentrations, is then also used to calculate the concentration of fixed groups on the IEM (See Section 2.2).

3.4. Electrosorption experiment

Two modes of operation were used in MCDI experiments. In batch mode operation, the salt solution was continuously fed into the flow channel at a flow rate of 40 ml min^{-1} from a 150 ml recycle reservoir, and returned to the same reservoir, for 15 min. A conductivity probe was placed in the reservoir to monitor the change in salt concentrations. During the adsorption step, a constant electrical voltage of 1.5 V was applied to the electrodes. The salt adsorption per cycle, Q ($\text{mmol}_{\text{salt}} \text{ g}_{\text{carbon}}^{-1}$), was calculated as

$$Q = \frac{1000 \cdot (C_{\text{initial}} - C_{\text{final}}) \cdot V_{\text{reservoir}}}{M_{\text{carbon}}} \quad (22)$$

where C_{initial} and C_{final} are the initial and final concentrations in the reservoir, $V_{\text{reservoir}}$ is the volume of the reservoir, and M_{carbon} is the total mass of carbon in the electrodes. During the desorption step, the voltage was reversed until the initial concentration was achieved in the recycle reservoir.

In the single-pass mode of operation, the feed solution passed through the cell at a flow rate of 20 ml min^{-1} and the conductivity of the effluent was monitored. The same charge and discharge voltages were applied. In this case, the salt adsorption per cycle is measured as:

$$Q = \frac{1000 \cdot \left(\int_0^{t_{\text{ads}}} (C_{\text{feed}} - C_t) \cdot dt \right) \cdot \dot{V}}{M_{\text{carbon}}} \quad (23)$$

where \dot{V} is the volumetric flow rate, C_{feed} is the feed salt concentration, C_t is the outlet salt concentration at any time t , and t_{ads} is the adsorption cycle duration.

In both adsorption and desorption steps, the charge consumption (σ) was determined by integrating the electrical current through the cell;

$$\sigma_{\text{ads/des}} = \int_0^{t_{\text{ads/des}}} I_e(t) \cdot dt \quad (24)$$

where t_{ads} and t_{des} are the duration of the adsorption and desorption cycles, respectively. Multiplying the charge consumption by cell voltage gives the energy consumption of each step. In addition, the charge efficiency (Λ) is defined as the moles of salts adsorbed/or released per moles of electron transferred

$$\Lambda_{\text{ads/des}} = \frac{\left(\frac{Q}{1000} \right) \cdot M_{\text{carbon}}}{\sigma_{\text{ads/des}} \cdot F} \quad (25)$$

The feed water recovery is another critical term which is defined as the ratio of the volumes of desalinated water produced to that of the feed over one full cycle;

$$\text{Water recovery} = \frac{\text{volume of desalted water produced during adsorption}}{\text{total volume of feed water}} \quad (26)$$

While the water productivity is given as:

$$\text{Water productivity} = \frac{\text{adsorption cycle time}}{\text{total cycle time (adsorption and desorption)}} \quad (27)$$

To determine the parameters required for the mD model, equilibrium

experiments were performed. In these sets of experiments, a constant voltage of 1.5 V was applied to the CDI cell operating in batch-mode until the concentration of salt in the recycle reservoir plateaued. At equilibrium, there is no ionic transport; which means, the applied voltage is only distributed over the EDL potential drops. This experiment was carried out at four different salt concentrations (ranging from 5 to 50 mM). Certain parameters of the model (μ_{att} , $C_{\text{St},0}$, and α), were adjusted to fit the modelling results of equilibrium salt adsorption and charge efficiency to that of the experimental data.

To collect the data for Section 4.5, the experiments were initially conducted by keeping the adsorption time constant at 15 min for all the feed concentrations and extending the desorption step as needed to ensure that all adsorbed ions were released back to the recycle reservoir. On the other hand, to investigate regeneration using a brine stream, desorption was performed using a separate recycle reservoir at a different initial concentration, (C_{initial}) which is greater than the original feed water concentration. The ratio of C_{initial} for each regeneration step to the original feed concentration is called the ‘brine to feed concentration ratio’. When desorption was complete, a quick air flush depleted the MCDI unit of any residual brine. Therefore the quality of water produced during the adsorption steps remained constant.

To determine the lag time in response and the minimum number of uniform sub-cells required for unit discretisation, the flow channel was characterised through the response to a pulse injection of dye. The method and relevant equations for this analysis are described in the Appendix E.

The activity coefficient of the ions Na^+ and Cl^- in the solution was computed using Aspen Plus V8.6 (Aspen One) employing the Pitzer thermodynamic model. The activity data was generated with respect to increasing ionic strength (from 0.01 to 0.3 M) at 25 °C.

MATLAB R2016a was utilised as the computational software to solve the set of equations discussed in Section 2. A block diagram of the sequence of parameter determination and mathematical calculation is depicted in Appendix F (see Fig. F1). A numerical approach was employed for optimization sequences in which the algorithms use the simplex search method of Lagarias et al. [31].

4. Results and discussion

4.1. Characterization of the MCDI cell

Initial experiments focused on determining the parameters needed for the MCDI model to be effective. The parameters determined experimentally for the carbon electrodes are summarized in Table 1. Details of the experimental procedures used to determine these parameters and further characterization details are provided in the Appendix D.

The permeability coefficient of the counter-ions (Na^+ in case of CMX and Cl^- in case of AMX) was measured using the method

Table 1
Summary of Parameters Determined Experimentally.

Carbon Electrodes		
Thickness (μm)		150 ± 15
Surface area ($\text{m}^2 \text{ g}^{-1}$)		540 ± 4
Micropore Size (nm)		0.7–1.5
Electrode Micropore Volume Fraction (%)		40
Electrode Macropore Volume Fraction (%)		30
Specific Capacitance (F g^{-1})		40
Ion Exchange Membranes		
Counter-ion Diffusion Coefficient ($D_{+,m}$) ($\text{m}^2 \text{ s}^{-1}$)	CMX	$(1.1 \pm 0.2) \times 10^{-11}$
	AMX	$(1.5 \pm 0.2) \times 10^{-11}$
Concentration of fixed charges ($C_{\text{fix},m}$) (mmol per litre of swollen membrane)	CMX	1148 ± 16
	AMX	1152 ± 56

explained in Section 3.2. The observed increase in H^+ and OH^- concentration in the salt chamber of the diffusion cell over more than 3 h can be found in Fig. D1. Results were obtained using the first hour of the data collected, where the rate of change is constant (see Table 1). The concentration of the fixed charges in the membrane (Table 1) and the partition coefficients under the experimental conditions (Table D1) was determined through the sorption experiment described in Section 3.2. At 10 mM of NaCl, the concentration of counter and co-ions in the CMX membrane were determined as 1149 ± 15 mM and 1.1 ± 0.7 mM, while that in the AMX were 1154 ± 54 mM and 1.7 ± 0.7 mM. While Kamcev et al. [26] employed a different type of IEM, the concentration of counter and co-ions in the membrane we obtained is comparable with their published results (1060 Na^+ and 0.1 Cl^- mmol per litre of swollen cation exchange membrane, and 1005 Cl^- and 0.08 for Na^+ mmol per litre of swollen anion exchange membrane, at the external concentration of 10 mM NaCl). It is noteworthy that they defined the concentration as moles of ion per volume of the water sorbed which needs to be converted to the volume of swollen membrane prior to comparison.

From these results, the diffusion coefficients can be obtained (see Table 1). CMX and AMX are mechanically rigid structures while the fixed charges on the IEMs contribute to strong electrostatic interactions. Hence, in comparison with the diffusion coefficients of the same ions in water, small values are expected (see Table 1). Utilizing a similar experimental approach, values with the same order of magnitude have been reported for monovalent ions diffusing through a range of cation/anion exchange membranes in the literature [32]. In addition, a smaller diffusivity coefficient of Na^+ through CMX relative to that of Cl^- through AMX was expected owing to the reduced ionic mobility of the former [33].

It is worth mentioning that while the permeability coefficients and sorption values are strong function of concentration, this effect is reduced for the diffusion coefficient. The values obtained here are thus taken as constant across all concentrations used in this work. While any mathematical modelling is constructed on some simplifying assumptions, the theoretical approach can be strengthened by accurate determination of model parameters. Prior mathematical approaches to MCDI modelling have neither provided any specific methodology for the measurement of the diffusion coefficients in the IEMs, nor justified the values selected [14,34]. By eliminating these estimations from the mathematical approach, the reliability of the MCDI model can be enhanced.

Finally, the response of the MCDI cell to a pulse input of dye was used to determine the lag time in response as well as the minimum number of spatially uniform regimes required for the model to account for dispersion effects. For the MCDI unit utilised in this work, at the lowest flowrate used in experiments (20 ml min^{-1}), there is a mean residence time of 67 s, a lag time of 14 s and a minimum of 2 sub-cells must be considered when discretising the computational domain of the flow channel. Mean residence time equals the volume of the flow channel divided by the volumetric flow rate. Further information, including the dimensionless age distribution, can be found in Appendix E (see Fig. E1).

4.2. Model validation

Equilibrium adsorption and desorption experiments of MCDI were first conducted at four different feed concentrations ranging from 5 to 50 mM to validate the mathematical model. The outcome of the validated model can then be compared with the performance of the MCDI unit under both batch and single-pass mode of operation. Fig. 2 (a) shows the typical concentration change in the recycle reservoir during one full cycle of batch mode adsorption and desorption while Fig. 2 (b) depicts the salt concentration of the effluent stream over single-pass mode of operation. This data was used to determine μ_{att} , $C_{St,0}$ and α by minimising the sum of squared errors (see

Table 2). Fig. 2 shows that there is a very good agreement between the model and the experimental data.

In the MCDI model developed in this work, the flux of co-ions through the ion-exchange membrane is ignored. This assumption was made following calculations which showed that the flux of co-ions was significantly smaller than the flux of counterions. This arises from very small concentration of co-ions in the IEMs. The contribution of the co-ions to the increase in salt concentration in the macropores of the carbon arises not from the flux of these ions electromigrating through the IEM, but rather from the repulsion of co-ions from the micropores upon applying an electrical voltage. During the initial period, both before a voltage is first applied and in the initial cycles where the membranes are reaching steady state, there is some leakage of co-ions into the macropores. This is both because the membrane is initially soaked in the co-ion/counter-ion mixture and retains some of these ions on its surface and because co-ion diffusion across the membrane during these initial cycles is high due to the stronger concentration gradient during this period. However, under the stable dynamic conditions of adsorption/desorption cycles of MCDI, the flow of co-ions is principally an exchange between the macro and micropores, rather than transport through the membrane [14,34]. The results of our model indeed show that during stable dynamic operation, the flux of co-ions repulsed from the carbon micropores during the adsorption cycle matches the flux of co-ions adsorbed during desorption.

The charge efficiency of MCDI treating a feed of 10 mM NaCl in single-pass mode (as depicted in Fig. 2 (b)) was experimentally measured at 94.9%. Considering that the co-ion flux is negligible, we strongly believe that the charge efficiency below 100% is attributed to other factors such as faradaic reactions due to carbon surface oxidation, and electromigration of hydronium and hydroxyl ions [35,36]. It is worth mentioning that these factors have not been considered in the MCDI theory employed in this work.

Additionally, given the diffusion coefficients of the CMX and AMX membranes measured and reported in Section 4.1, the potential drop over the cation-exchange membrane is found to be higher than that of the anion-exchange membrane. This result is consistent with the fact that the CMX membrane has greater electrical resistance compared with the AMX one [37]. To maintain the electroneutrality in the spacer compartment, the flux of Cl^- migrating through the AMX must be equal to the flux of Na^+ migrating through the CMX and so the potential drops over these two ion exchange member are unequal. To date, no MCDI model has identified and included this effect.

4.3. Regeneration of MCDI cell using a brine stream

The validated model was now used to investigate whether a higher concentration of brine could be used for MCDI regeneration. To answer this question, we first studied the effect of the brine to feed concentration ratio on regeneration duration and feed water recovery during batch operation, using both experiments and modelling. Fig. 3(a) and (b) show the increase in desorption time with increasing concentration of the brine stream for initial feed water salt concentrations of 5 and 10 mM, respectively using batch operation. The ions adsorbed in the EDLs of carbon micropores are repulsed once the cell voltage is reversed and transfer back to the macropore voids and then diffuse through the ion-exchange membrane to get to the flow channel. Referring back to Eq. (5), the concentration difference on both sides of the membrane contributes to the flux of ions diffusing through this layer. It is apparent that by increasing the concentration of the brine regeneration stream, the flux of ions decreases, and consequently, desorption time extends. It is not practical to spend more time on regenerating the operation unit than the time used to produce fresh water. As a result, further increasing the brine to feed ratio above 4, would not be practical in the present case.

The solid line in Fig. 3(a) and (b) demonstrates that the desorption time obtained from the mathematical model at different brine to feed

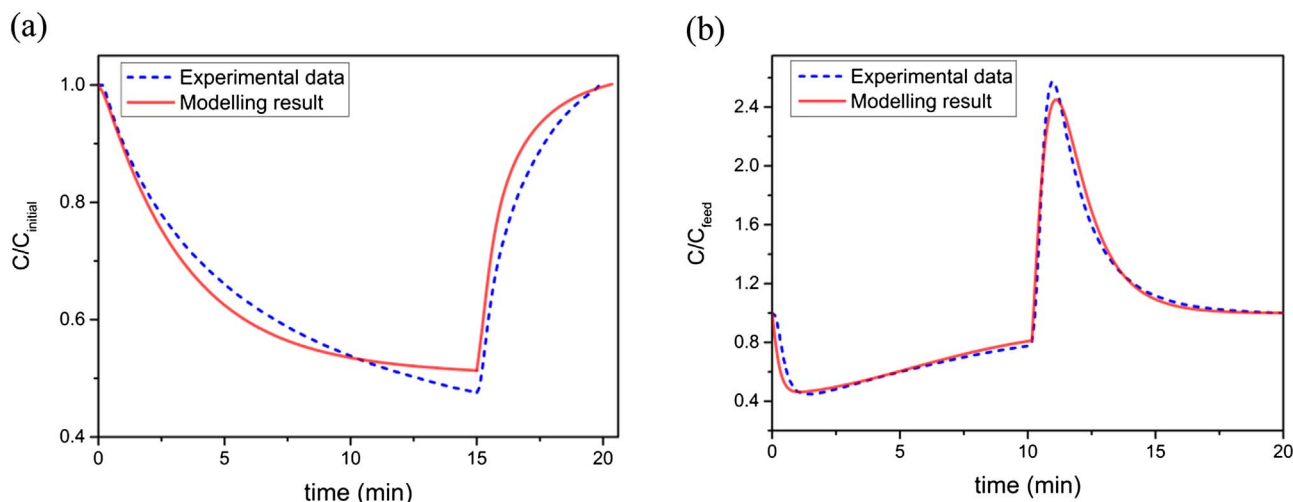


Fig. 2. Ion transport model validation, Molar concentration of NaCl solution (a) as a proportion of the initial concentration (10 mM) in the recycle reservoir as a function of time during batch-mode MCDI, (b) as a proportion of the feed concentration (10 mM) during single-pass mode MCDI vs time.

Table 2
List of parameters determined from model optimization.

μ_{att}	dimensionless physical attraction potential	1.8 ± 0.2
$C_{St,0}$	Stern layer capacitance at zero cell voltage	$(3.2 \pm 0.4) \times 10^8 \text{ F m}^{-3}$
α	charge dependency coefficient of the Stern layer capacity	$16 \pm 2 \text{ F m}^3 \text{ mol}^{-2}$

concentration ratios is consistent with the experimental data, as can only be achieved when a comprehensive ion transport model is employed.

To further investigate the desorption performance with more concentrated brines in batch operation, we calculated the water recovery considering the fact that water can be saved by re-using the brine stream. The water recovery in this case is shown in Fig. 4(a) and (b) employing the experimental data points represented in Fig. 3(a) and (b), respectively. The water recovery initially increases due to a reduction in feed water used for regeneration but falls at higher brine concentrations due to the extension in the desorption time. Under the operational conditions given in Section 3.3, the optimal water recovery

occurs when the brine stream is around twice the initial feed concentration (either 5 or 10 mM).

For industrial applications, the MCDI unit will generally be used in a single-pass mode. Fig. 5(a) depicts the conventional single-pass operation mode where the same brackish water feed is fed into the MCDI cell both during adsorption and desorption. However, utilizing the same concepts as described above, we proposed a set-up with a separate regeneration recycle tank as illustrated in Fig. 5(b). In this case, the effluent stream produced during regeneration can be collected and partially re-used for the next desorption step. By adding a feed-and-bleed feature to this regeneration tank, we can keep the concentration at a specific level to maximize water recovery. Although this concentration is higher than the feed, regeneration is still practical.

The water recovery and productivity for the configuration depicted in Fig. 5(b) is shown in Fig. 6 as a function of the ratio of the concentration in the regeneration recycle tank to the concentration of the feed. As described in Section 3.4, water productivity is determined as the time the MCDI set-up is under operation for desalted water production to the total time spent on adsorption and desorption. To obtain this data, the mathematical approach explained earlier was employed in a single-pass mode (adsorption with 10 mM NaCl solution as the brackish feed water, and desorption assuming a constant

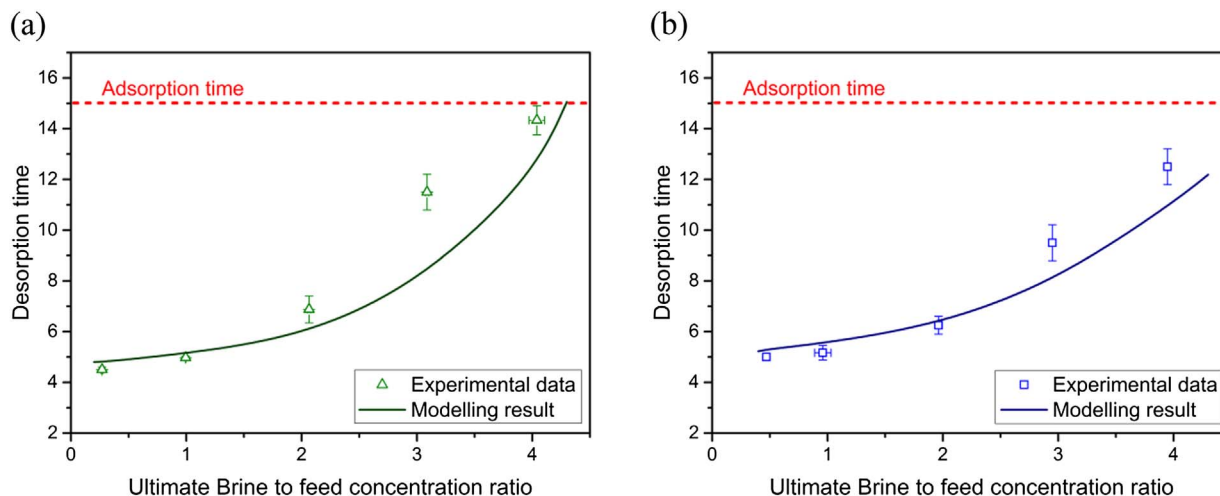


Fig. 3. The effect of brine concentration on desorption time in a batch-mode operation of MCDI, (a) Initial concentration of 5 mM, (b) initial concentration of 10 mM. The solid line represents modelling result.

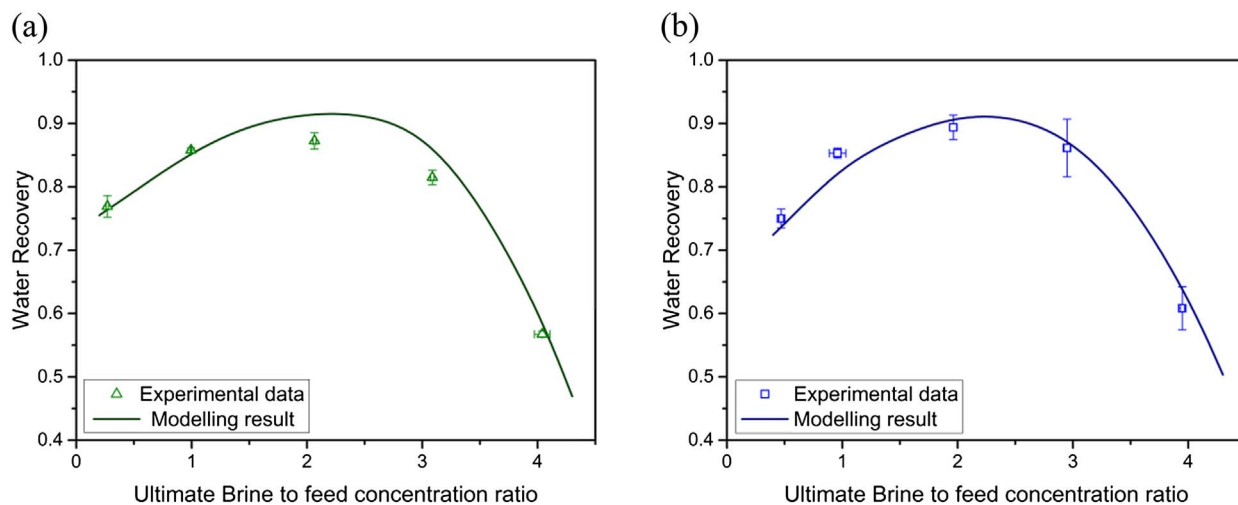


Fig. 4. The effect of ultimate brine to feed concentration ratio on water recovery (a) Initial concentration of 5 mM, (b) initial concentration of 10 mM. The adsorption time was kept constant at 15 min.

concentration in the regeneration recycle tank). For each case, the desorption step was maintained for sufficient time to release all the adsorbed ions back into the regeneration recycle tank. This was determined mathematically by equating the area above the regeneration tank concentration versus time curve during desorption to the area under the feed concentration versus time curve during adsorption. Recycling the brine stream improves water recovery by 47% at 20 ml min⁻¹ and 43% at 40 ml min⁻¹ desorption flow rate in comparison with the conventional operating mode (Fig. 6). As expected, water productivity drops since the desorption time is prolonged.

The energy consumption per cycle does not change significantly since the total amount of adsorbed salt is maintained constant within each adsorption step. This is not consistent with the recent publication by García-Quismondo et al. [15], who observed an enhancement in energy efficiency when a concentrated brine stream was used during regeneration. These discrepancies may arise due to the definition of energy efficiency used by them and due to the different operational modes used.

In the recent review article written by Suss et al. [16], the authors briefly suggested that water recovery of CDI systems might be enhanced

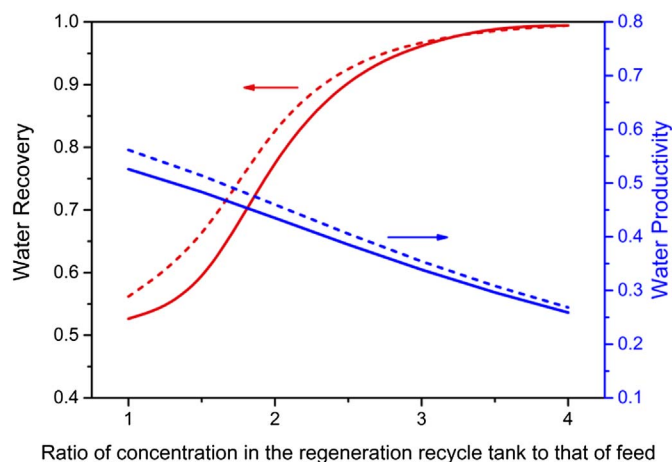


Fig. 6. Water recovery and productivity at different ratios of concentration in the regeneration recycle tank to that of the feed. Flow rate at desorption is set at 20 ml min⁻¹ for the solid line and 40 ml.min⁻¹ for the dashed line.

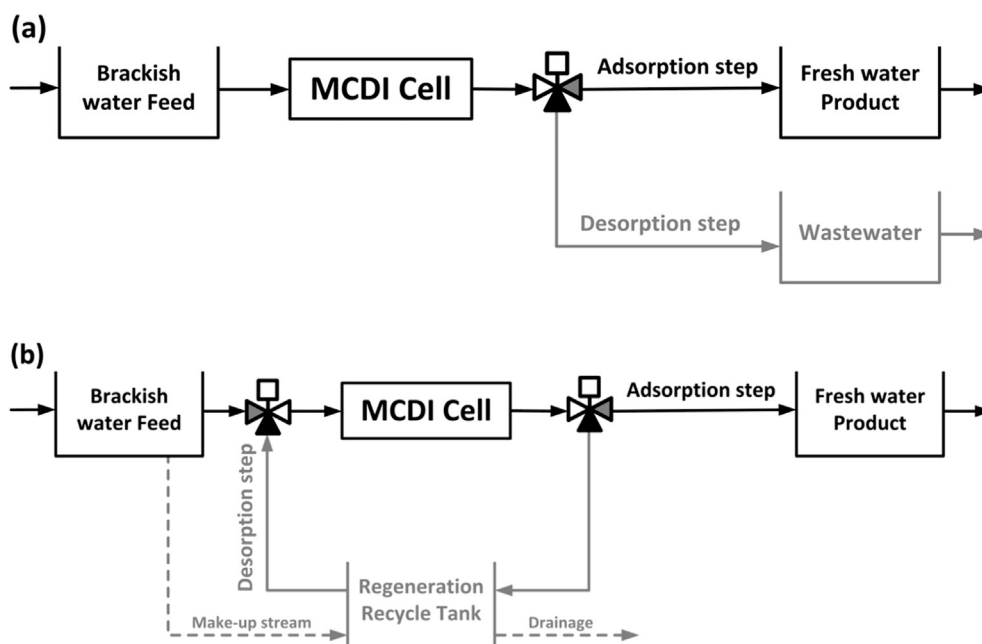


Fig. 5. MCDI set-up, (a) conventional operational mode, (b) with addition of regeneration recycle tank. Grey line demonstrates the flow direction during desorption step.

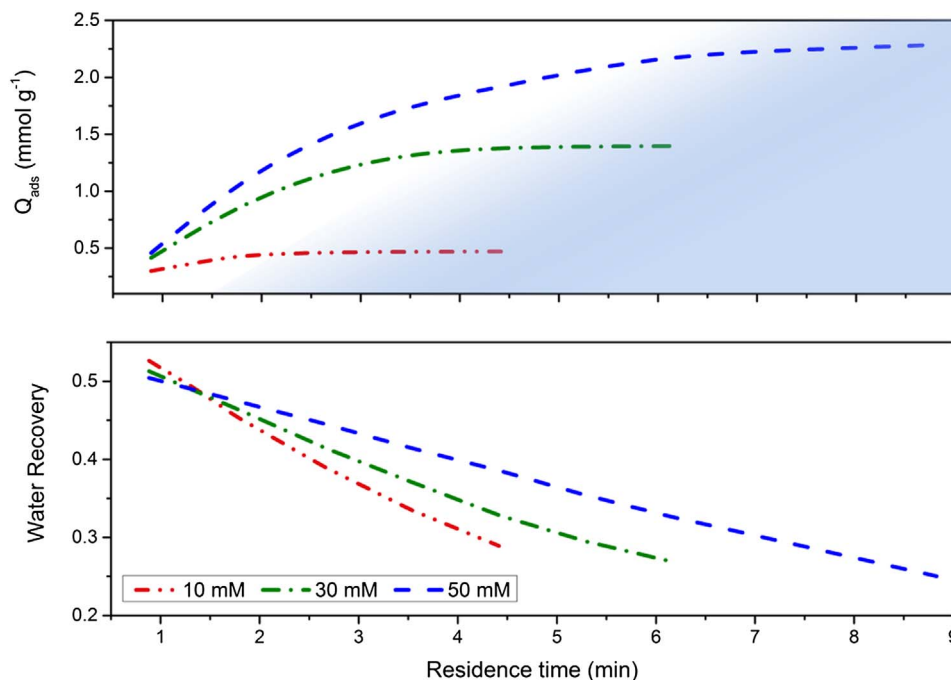


Fig. 7. Variation in salt adsorption and water recovery as the residence time in the MCDI unit is increased. The cell width and all other operating conditions were kept constant.

through *brine management*. The outcome of this section, has answered this important question as to whether or not a brine stream can be re-circulated.

It is noteworthy that the concentration of the stream leaving the MCDI cell varies with time. Therefore, the input to the regeneration recycle tank is not at constant concentration over the desorption period. However, it is more practical, from an industrial point of view, to maintain the flow rate from this tank and the tank concentration at a certain value. In practice, this would be achieved by utilizing a large regeneration tank volume and by varying the flowrate of feedwater diverted into the tank over time.

4.4. Determination of optimum residence time in the MCDI unit

In dealing with high salinity brackish water, one might be tempted to simply increase the residence time in the MCDI unit to provide sufficient salt adsorption. In this work, we aimed to investigate whether or not there is a limit to the residence time in a MCDI unit beyond which performance falls, using the mathematical model. This information is vital to effective design of MCDI systems. To increase residence time one can increase the length of the MCDI unit in the direction of flow, or decrease the volumetric flow rate. As shown in Fig. 7, increasing the residence time in the cell in this manner (while maintaining a constant adsorption cycle time) leads to greater maximum desalination capacity only to a certain extent, with Q_{ads} eventually reaching a plateau. Further increases in unit length or reductions in flowrate are not advantageous. Water recovery also declines continuously by increasing the residence time. As an example, for a feed of 10 mM, increasing this time from 2.7 min to 4.4 min results in a 10% fall in water recovery while the increase in salt adsorption per cycle is limited to 1%. The result is comparable if the adsorption cycle time is extended proportionally with the residence time in the MCDI cell. Similarly in this case, after a certain residence time in the MCDI unit, the rate at which salt adsorption grows is small in comparison with the rate at which water recovery drops.

To understand this effect further, Fig. 8 shows the concentration of the electrolyte solution in the flow channel during regeneration, as a function of time and position along a unit of 0.2 m length at 10 mM feed concentration. This Figure shows that the salt concentration reaches a significantly higher concentration towards the end of the unit than in the entrance region, owing to ions being released back to the stream. That is, towards the end of the unit, the brine to feed concentration

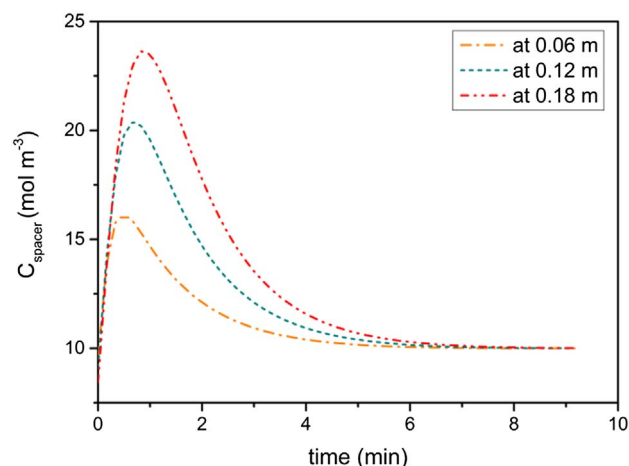


Fig. 8. C_{spacer} versus time during desorption at 0.06, 0.12 and 0.18 m along the MCDI unit under conventional single-pass mode of operation at 10 mM feed concentration.

ratio is much higher. Extended regeneration time is then inevitable as discussed in Section 4.5.

5. Conclusion

In this work, we have investigated whether or not a brine stream, which is more concentrated than the feed solution, is capable of regenerating a MCDI unit and whether there is an optimum residence time. To date, no other research group has tackled these important research questions.

To approach these problems, we first extended the MCDI model available in the literature, to specifically account for the activity coefficients of the counter-ions and co-ions within the membranes themselves. Further, we used additional independent experiments to determine the diffusion coefficients within these membranes. Importantly, these experiments allowed for an improved model, where the voltage drop across the cation exchange membrane was greater, due to the lower ionic mobility of Na^+ in comparison with Cl^- . The

extension of the model to include these features has not been reported to date in the field of MCDI. Further, the use of the revised model resulted in a good fit between the model and experimental data, with only three adjustable parameters.

The combined use of the revised model with batch experiments demonstrated that there is a trade-off between the increase in water recovery from the re-use of brine and the decrease in water productivity owing to desorption time extension. We showed that a brine to feed concentration ratio of around two provided optimum performance in a batch mode. Over 40% enhancement in water recovery could be achieved by recycling brine in continuous operation, but the optimum brine to feed ratio depended upon the relative importance of water recovery and productivity.

In the last part of this study, we again employed the mathematical model to determine the optimal residence time in the MCDI unit. By increasing the length of the unit, and proportionally the adsorption time, we observed a trade-off between the enhancement in desalination capacity and a fall in water recovery. Residence times beyond a certain value were ineffective under the process conditions employed here.

Acknowledgements

Armineh Hassanvand acknowledges The University of Melbourne

Appendix A. Manning's counter-ion condensation theory

Assuming that the ion-exchange membrane behaves similarly to a polyelectrolyte solution, Manning's counter-ion condensation theory can be employed to determine the activity coefficients in the IEM. For a 1:1 salt, the activity coefficient of the counter and co-ions in the ion-exchange membrane can be estimated from Eq. (A.1) and (A.2), respectively.

$$\gamma_{+,m} = \frac{\frac{1}{\xi} \frac{C_{fix,m}}{C_{-,m}} + 1}{\frac{C_{fix,m}}{C_{-,m}} + 1} \exp \left[-\frac{\frac{1}{2} \frac{C_{fix,m}}{C_{-,m}}}{\frac{C_{fix,m}}{C_{-,m}} + 2\xi} \right] \quad (A.1)$$

$$\gamma_{-,m} = \exp \left[-\frac{\frac{1}{2} \frac{C_{fix,m}}{C_{-,m}}}{\frac{C_{fix,m}}{C_{-,m}} + 2\xi} \right] \quad (A.2)$$

where ξ is the dimensionless linear charge density of the polyelectrolyte chain with values between 1 and 4 [26]. Kamcev et al. [26] has estimated the value of ξ for three cation and anion exchange membranes across a range of salt concentrations. A typical value of 2 is used in this work.

Appendix B. Electrode characterization

Scanning electron microscope (SEM) images of the electrodes were obtained using a Jeol JSM-7001F scanning electron microscope. All samples

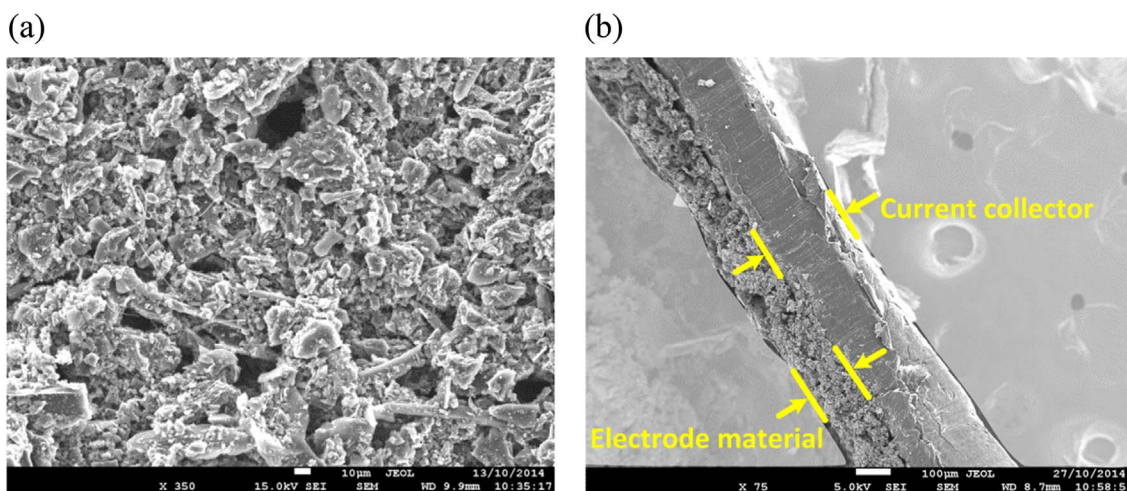


Fig. B1. SEM images of activated carbon electrodes, (a) surface and (b) cross-section views.

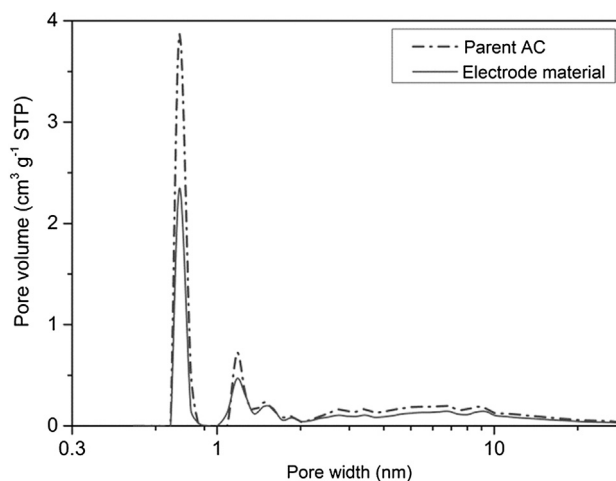


Fig. B2. Pore size distribution determined from the DFT method. Dash-dot line: Norit SA4 as the parent source of activated carbon, and solid line: Electrode material prepared as powder.

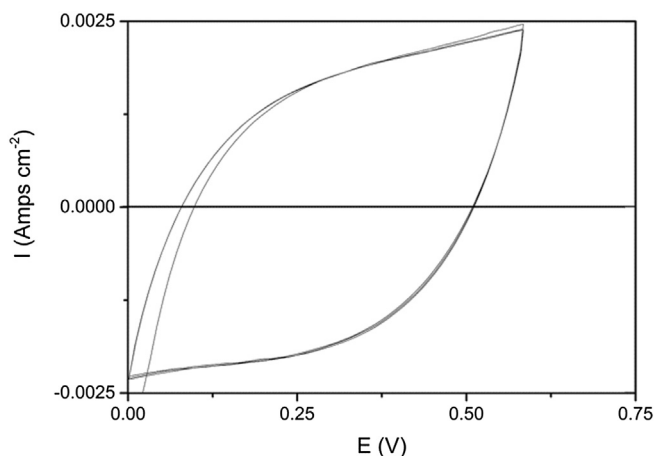


Fig. B3. Cyclic voltammetry (scan rate of 5 mV/s) for the AC electrode in 1 M NaCl solution.

were sputter coated with Iridium prior to imaging and the instrument was operated at 15 kV at a working distance of 10 mm. A surface and pore size analyser (Micromeritics ASAP 2010) was used to determine the nitrogen adsorption-desorption isotherm. The specific surface area and pore size distributions were obtained from these isotherms using Brunauer-Emmett-Teller (BET) and Density Functional Theory (DFT) methods, respectively. The electrochemical performance of the AC electrodes was investigated with cyclic voltammetry (CV) using a potentiostat (Solatron 1287) equipped with Corware software. CV was conducted in a three-electrode system in which the carbon electrode, a graphite sheet, and an Ag/AgCl electrode were used as the working, the counter and the reference electrodes, respectively.

SEM images shown in Fig. B1 depict the surface and cross-section views of the carbon electrode. As shown in Fig. B1(a), the slurry has been cast uniformly on the graphite sheet which yields physical stability. The strong contact between carbon layer and graphite is indicative of sufficient usage of PVDF as the adhesive binder. Micropore volume fraction of the electrode material, determined using the DFT method, is 55% (Fig. B2). Such a microporous structure leads to the electrical double layer overlapping inside the pores. It is noteworthy that in the calculation of electrode micropore volume fraction, the voidage of the electrode was also considered. Φ values employed in the theoretical model are corresponding to the *electrode* micro and macro pore volume fractions.

The CV curve of the AC electrodes is plotted in Fig. B3. The specific capacitance of the electrode was quantified to be 40 F g^{-1} at a scan rate of 5 mV/s. The rectangularity of the CV curves is indicative of ideal capacitor behavior [38] while the symmetry of the curves indicates pure electrosorption and desorption, with no Faradaic reactions occurring on the electrode surface [38], validating the assumption used in Section 2.

Appendix C. MCDI set-up

A schematic diagram of the MCDI set-up in batch mode operation and all the layers placed inside the poly(carbonate) frame are depicted in Fig. C1.

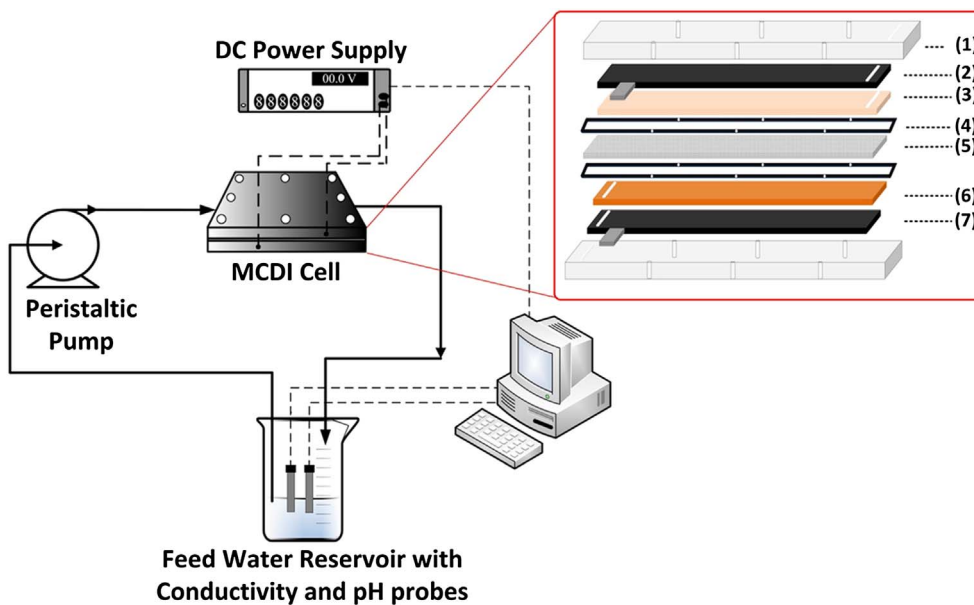


Fig. C1. Schematic diagram of the MCDI cell and set-up in batch mode operation. Within the MCDI cell, (1) poly(carbonate) frame, (2) carbon electrode (anode), (3) anion-exchange membrane, (4) silicon gasket, (5) spacer, (6) cation-exchange membrane, (7) carbon electrode (cathode).

Appendix D. Permeability test conducted on ion-exchange membranes

The permeability coefficient of the counter-ions (Na^+ in case of CMX and Cl^- in case of AMX) was measured using the method explained in Section 3.3. The observed increase in H^+ and OH^- concentration in the salt chamber of the diffusion cell over > 3 h can be found in Fig. D1. The permeability coefficients were obtained using the first hour of the data collected, where the rate of change is constant (see Table D1).

Table D1

Permeability coefficients and Partition Coefficients of counter and co-ions in IEMs.

Co-ion Diffusion Coefficient ($D_{-,m}$) ($\text{m}^2 \text{s}^{-1}$)	CMX	$(5 \pm 2) \times 10^{-12}$
	AMX	$(3 \pm 1) \times 10^{-11}$
Counter-ion Permeability Coefficient ($P_{+,m}$) ($\text{m}^2 \text{s}^{-1}$)	CMX	$(1.3 \pm 0.2) \times 10^{-9}$
	AMX	$(1.5 \pm 0.2) \times 10^{-9}$
Co-ion Permeability Coefficient ($P_{-,m}$) ($\text{m}^2 \text{s}^{-1}$)	CMX	$(5.4 \pm 0.8) \times 10^{-13}$
	AMX	$(5.7 \pm 0.5) \times 10^{-12}$
Counter-ion Partition Coefficient ($K_{+,m}$) ^a	CMX	117 ± 2
	AMX	101 ± 6
Co-ion Partition Coefficient ($K_{-,m}$) ^a	CMX	0.11 ± 0.07
	AMX	0.17 ± 0.07

^a The unit of partition coefficients is (mol per litre of swollen membrane / mol per litre of external solution).

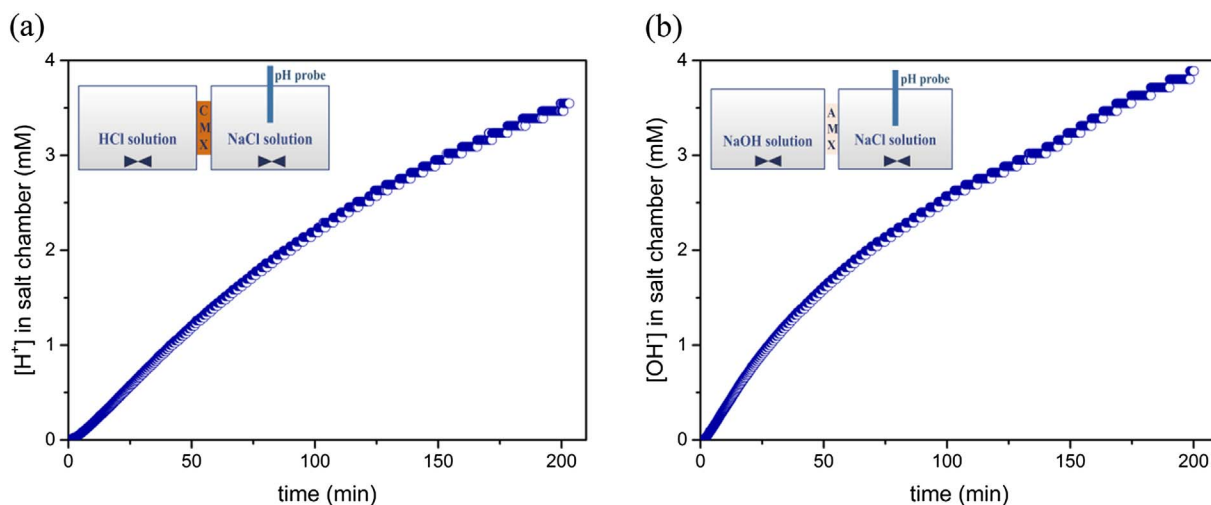


Fig. D1. Measured H^+ and OH^- concentrations in the salt chamber of the diffusion cell, used to determine the diffusivity coefficients of Na^+ and Cl^- in the CMX and AMX, respectively. The initial concentrations of all solutions were set at 10 mM.

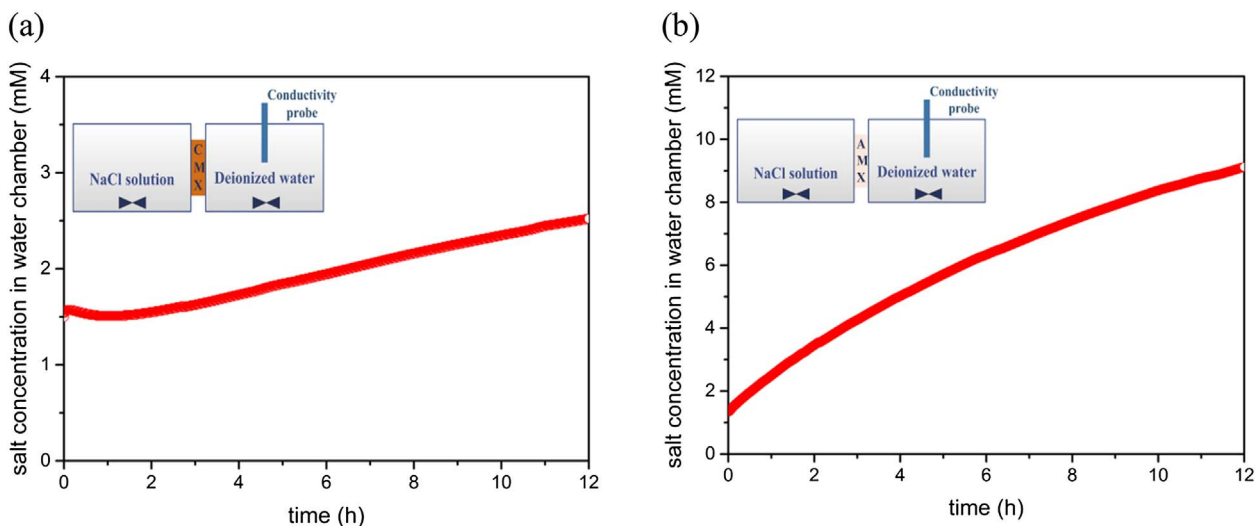


Fig. D2. Measured salt concentrations in the water chamber of the diffusion cell, used to determine the diffusivity coefficients of co-ions in the CMX and AMX, respectively. The initial concentrations of salt solutions were set at 10 mM.

Conversely, the increase in the salt concentration due to the permeation of the co-ions through CMX and AMX is illustrated in Fig. D2(a) and (b), respectively. The permeability coefficient of the co-ion is collected over the first 3 h of the data collection due to the slower rate of co-ion transport.

Appendix E. Flow channel characterization

The response to a pulse injection to the feed enables the residence time distribution of the MCDI unit to be determined. Using the N-tanks in series model, the number of mixed flow unit cells that are needed to describe the MCDI system can then be evaluated [39]. While water was flowing through the MCDI cell at a flow rate of 20 ml min⁻¹, 1 mM Methylene blue solution, was injected into the inlet of the unit in a very short interval of time. The tracer concentration in the exit stream (C_{effluent}(t)) was measured using corresponding calibration line for methylene blue conductivity versus its concentration. This concentration was then used to determine the mean residence time (\bar{t}) and variance (σ^2), and thus the dimensionless age distribution (E_θ) and the number of mixed flow unit cells (N) (Eqs. (E1)–(E3)).

$$\bar{t} = \frac{\int_0^\infty t \cdot C_{effluent}(t) \cdot dt}{\int_0^\infty C_{effluent}(t) \cdot dt}, \sigma^2 = \frac{\int_0^\infty t^2 \cdot C_{effluent}(t) \cdot dt}{\int_0^\infty C_{effluent}(t) \cdot dt} - \bar{t}^2 \tag{E1}$$

$$E_\theta = \frac{C_{effluent}}{\int_0^\infty C_{effluent}(t) \cdot dt}, \bar{t}, \theta = \frac{t}{\bar{t}} \tag{E2}$$

$$\sigma_0^2 = \frac{\sigma^2}{\bar{t}^2} = \frac{1}{N} \tag{E3}$$

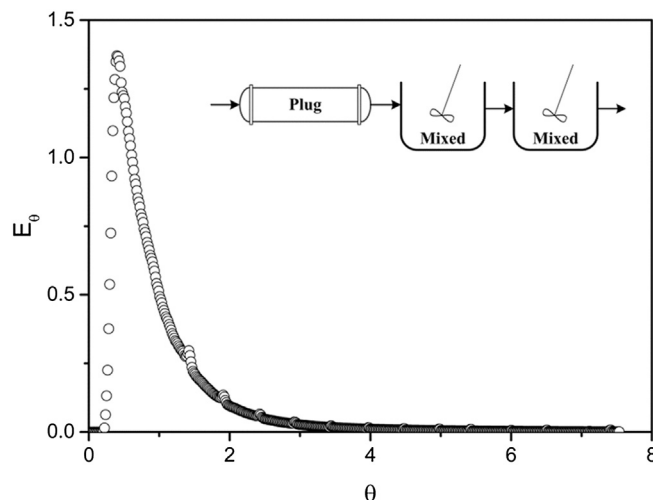


Fig. E1. The respond to the pulse injection of 1 mM Methylene blue solution to the inlet of MCDI cell at a flow rate of 20 ml min⁻¹. Corresponding compartment model is presented on top right corner.

First, from tracer injection, the mean residence time was obtained as 67 s using Eq. (E1). Then the dimensionless age distribution E_θ versus dimensionless time θ , shown in Fig. 1, suggests that the MCDI cell used in this work is behaving similar to a plug flow reactor followed by two mixed flow cells. The lag time in the early stages of E_θ corresponds to a plug flow reactor with no axial mixing with a residence time of 14 s. Then the subsequent number of fully-mixed tanks determines the minimum number of unit cells to be considered in the mathematical approach. To ensure the outcome of this experiment is applicable to all flow rates, the lowest flow rate used in the experimental work was selected to collect the resident time distribution data. It is apparent that at lower flow rates, E_θ expands, which corresponds to greater axial dispersion. Hence, it is crucial to obtain the response to the pulse input at the lowest operating flow rate for each MCDI unit to extract the minimum number of cells (N) required for modelling.

This experiment demands special care to make sure that the total amount of the tracer entering the system eventually leaves the cell. Otherwise, the RTD result will be affected by adsorption of the tracer on the carbon particles or the ion-exchange membranes. This was the case in the present work.

Appendix F. Modelling sequence

Modelling sequence explained in Sections 2.4 and 3.4 is summarized in Fig. F1.

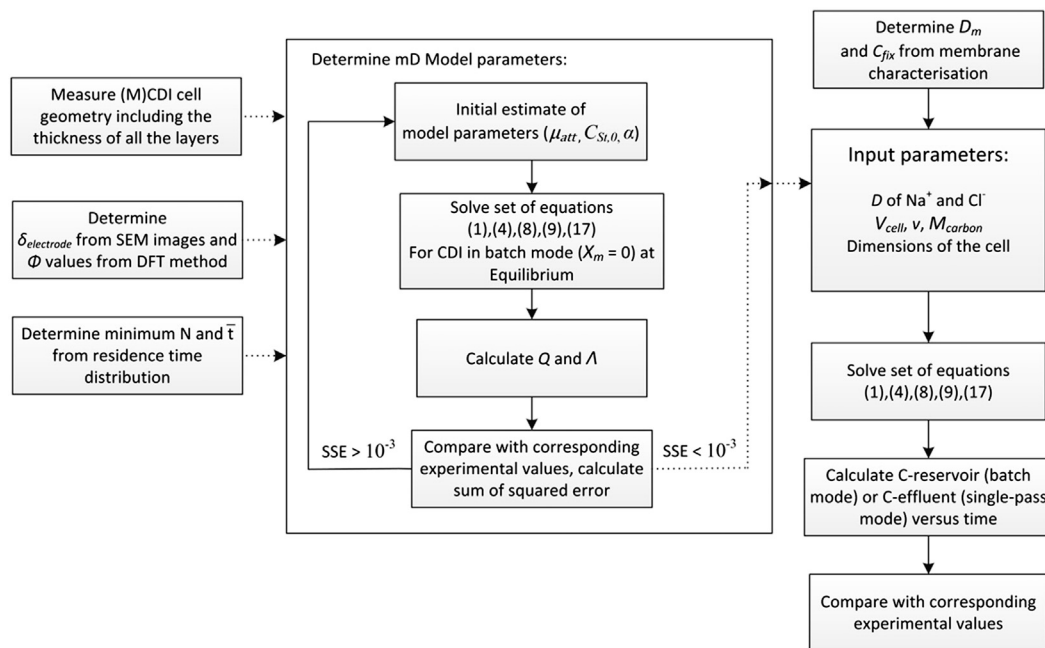


Fig. F1. Sequence of input parameter determination and mathematical modelling.

List of Symbols

a	activity	[mol m ⁻³]
A	orifice area of the diffusion cell	[m ²]
C	concentration	[mol m ⁻³]
C _{charge}	cation and anion concentration difference	[mol m ⁻³]
C _{St,0}	Stern layer capacitance at zero voltage	[F m ⁻³]
D	diffusion coefficient	[m ² s ⁻¹]
e	electrical charge of an electron	1.602 × 10 ⁻¹⁹ [C]
E	age distribution function	
F	Faraday Constant	96,487 [C mol ⁻¹]
I	current density	[A m ⁻²]
I _e	electrical current passing through the cell	[A]
J _{iy}	flux of ion i per area of the IEM in y direction	[mol s ⁻¹ m ⁻²]
K	partition coefficient	–
k _B	Boltzmann constant	1.38 × 10 ⁻²³ [m ² kg s ⁻² K ⁻¹]
M _{carbon}	mass of carbon material in one pair of the electrodes	[g]
N	number of sub-cells in the mathematical approach	–
P	permeability	[m ² s ⁻¹]
Q	salt adsorption per cycle	[mmol _{salt} g _{carbon} ⁻¹]
t	time	[s]
t̄	residence time	[s]
T	absolute temperature	[K]
v	velocity in the flow channel	[m s ⁻¹]
V _{cell}	electrical potential applied to the MCDI unit	[V]

V	volume	[m ³]
\dot{V}	volumetric flow rate	[m ³ s ⁻¹]
V _T	thermal voltage ($k_B T/e$)	25.5 [mV]
z	valency	–
Greek letters		
α	charge dependency coefficient of the Stern layer capacity	[F m ³ mol ⁻²]
γ	activity coefficient	–
δ	thickness	[m]
$\Delta\varphi$	dimensionless potential drop	–
θ	dimensionless time	–
κ	equivalent conductance	[S m ⁻¹]
Λ	charge efficiency	–
μ_{att}	dimensionless physical attraction potential	–
σ	charge consumption	[A s]
σ^2	variance of residence time distribution	[s ²]
Φ	volume fraction	–
Ψ	electrical potential	[V]
Subscripts		
+	counter-ion	
–	co-ion	
ads/des	adsorption or desorption step	
bulk	adjacent aqueous solution	
Diff	due to diffusion	
Don	Donnan potential	
final	final condition of the recycle reservoir	
fix	fixed charges on the ion-exchange membrane	
i	refers to ion type i	
initial	initial condition of the recycle reservoir	
m	membrane	
Ma	macropores of carbon	
me	membrane/electrode interface	
Mi	micropores of carbon	
ms	membrane/spacer interface	
reservoir	recycle reservoir in the batch-mode experiment	
spacer	flow channel compartment	
St	Stern layer	
Superscripts		
–	average value	
sol	solution	

References

- [1] A. Subramani, J.G. Jacangelo, Emerging desalination technologies for water treatment: a critical review, *Water Res.* 75 (2015) 164–187.
- [2] F.A. AlMarzooqi, et al., Application of capacitive deionisation in water desalination: a review, *Desalination* 342 (2014) 3–15.
- [3] Y. Oren, Capacitive deionization (CDI) for desalination and water treatment — past, present and future (a review), *Desalination* 228 (1–3) (2008) 10–29.
- [4] X. Gao, et al., Complementary surface charge for enhanced capacitive deionization, *Water Res.* 92 (2016) 275–282.
- [5] P.M. Biesheuvel, M.E. Suss, H.V.M. Hamelers, Theory of water desalination by porous electrodes with fixed chemical charge. arXiv.org, e-Print Arch, *Condens. Matter* (2015) 1–10.
- [6] S. Porada, et al., Review on the science and technology of water desalination by capacitive deionization, *Prog. Mater. Sci.* 58 (8) (2013) 1388–1442.
- [7] P.M. Biesheuvel, A. van der Wal, Membrane capacitive deionization, *J. Membr. Sci.* 346 (2) (2010) 256–262.
- [8] B.M. Asquith, J. Meier-Haack, B.P. Ladewig, Poly(arylene ether sulfone) copolymers as binders for capacitive deionization activated carbon electrodes, *Chem. Eng. Res. Des.* 104 (2015) 81–91.
- [9] R. Zhao, et al., Energy consumption in membrane capacitive deionization for different water recoveries and flow rates, and comparison with reverse osmosis, *Desalination* 330 (0) (2013) 35–41.
- [10] A. Omosebi, et al., Asymmetric Electrode Configuration for Enhanced Membrane Capacitive Deionization, *ACS Appl. Mater. Interfaces* (2014) (Ahead of Print).
- [11] C. Wang, et al., Parameter optimization based on capacitive deionization for highly efficient desalination of domestic wastewater biotreated effluent and the fouled electrode regeneration, *Desalination* 365 (2015) 407–415.
- [12] Y. Liu, et al., Review on carbon-based composite materials for capacitive deionization, *RSC Adv.* 5 (20) (2015) 15205–15225.
- [13] I. Villar, et al., Carbon materials as electrodes for electrosorption of NaCl in aqueous solutions, *Adsorption* 17 (3) (2011) 467–471.
- [14] R. Zhao, et al., Optimization of salt adsorption rate in membrane capacitive deionization, *Water Res.* 47 (5) (2013) 1941–1952.
- [15] E. Garcia-Quismondo, et al., New operational modes to increase energy efficiency in capacitive deionization systems, *Environ. Sci. Technol.* 50 (11) (2016) 6053–6060.
- [16] M. Suss, et al., Water desalination via capacitive deionization: what is it and what can we expect from it? *Energy Environ. Sci.* 8 (8) (2015) 2296–2319.
- [17] P.M. Biesheuvel, et al., Theory of membrane capacitive deionization including the effect of the electrode pore space, *J. Colloid Interface Sci.* 360 (1) (2011) 239–248.
- [18] P.M. Biesheuvel, et al., Attractive forces in microporous carbon electrodes for capacitive deionization, *J. Solid State Electrochem.* 18 (5) (2014) 1365–1376.
- [19] S. Porada, et al., Effect of electrode thickness variation on operation of capacitive deionization, *Electrochim. Acta* 75 (0) (2012) 148–156.
- [20] T. Kim, et al., Enhanced charge efficiency and reduced energy use in capacitive deionization by increasing the discharge voltage, *J. Colloid Interface Sci.* 446 (2015) 317–326.
- [21] W. Tang, et al., Investigation of fluoride removal from low-salinity groundwater by single-pass constant-voltage capacitive deionization, *Water Res.* 99 (2016) 112–121.
- [22] S. Porada, et al., Water desalination using capacitive deionization with microporous carbon electrodes, *ACS Appl. Mater. Interfaces* 4 (3) (2012) 1194–1199.
- [23] T. Sata, Ion exchange membranes: preparation, characterization, modification and application, Royal Society of Chemistry, 2004.
- [24] F.G. Helfferich, Ion exchange, Courier Corporation, 1962.
- [25] J. Mackie, P. Meares, The diffusion of electrolytes in a cation-exchange resin membrane. I. Theoretical, *Proceedings of the Royal Society of London A*:

- Mathematical, Physical and Engineering Sciences, The Royal Society, 1955.
- [26] J. Kamcev, D.R. Paul, B.D. Freeman, Ion activity coefficients in ion exchange polymers: applicability of Manning's Counterion condensation theory, *Macromolecules* 48 (21) (2015) 8011–8024.
- [27] A.A. Sonin, R.F. Probstein, Hydrodynamic theory of desalination by electro dialysis, *Desalination* 5 (3) (1968) 293–329.
- [28] R.A. Robinson, R.H. Stokes, *Electrolyte Solutions*, [Electronic Resource] the Measurement and Interpretation of Conductance, Chemical Potential, and Diffusion in Solutions of Simple Electrolytes, 2d, London, Butterworths, 1970 [1965, reprinted 1970]. ed., rev.
- [29] H. Strathmann, *Ion-exchange membrane separation processes*, 9 Elsevier, 2004.
- [30] G.M. Geise, B.D. Freeman, D.R. Paul, Sodium chloride diffusion in sulfonated polymers for membrane applications, *J. Membr. Sci.* 427 (2013) 186–196.
- [31] J.C. Lagarias, et al., Convergence properties of the Nelder-Mead simplex method in low dimensions, *SIAM J. Optim.* 9 (1) (1998) 112–147.
- [32] H. Miyoshi, Diffusion coefficients of ions through ion-exchange membranes for Donnan dialysis using ions of the same valence, *Chem. Eng. Sci.* 52 (7) (1997) 1087–1096.
- [33] A. Heintz, E. Wiedemann, J. Ziegler, Ion exchange diffusion in electromembranes and its description using the Maxwell-Stefan formalism, *J. Membr. Sci.* 137 (1) (1997) 121–132.
- [34] R. Zhao, P.M. Biesheuvel, A. van der Wal, Energy consumption and constant current operation in membrane capacitive deionization, *Energy Environ. Sci.* 5 (11) (2012) 9520–9527.
- [35] B. Shapira, E. Avraham, D. Aurbach, Side reactions in capacitive deionization (CDI) processes: the role of oxygen reduction, *Electrochim. Acta* 220 (2016) 285–295.
- [36] X. Gao, et al., Capacitive deionization using alternating polarization: effect of surface charge on salt removal, *Electrochim. Acta* 233 (2017) 249–255.
- [37] P. Długołęcki, et al., Transport limitations in ion exchange membranes at low salt concentrations, *J. Membr. Sci.* 346 (1) (2010) 163–171.
- [38] J. Lee, et al., Hybrid capacitive deionization to enhance the desalination performance of capacitive techniques, *Energy Environ. Sci.* 7 (11) (2014) 3683–3689.
- [39] O. Levenspiel, *Chemical Reaction Engineering*, third ed., Wiley, 1998 (656 pp).